

**X-ray absorption spectroscopy study of valence and site occupation of copper in  $\text{LiNbO}_3:\text{Cu}$** 

Tonya Vitova\* and Josef Hormes

*Institute of Physics, University of Bonn, Nußallee 12, D-53115 Bonn, Germany*

Konrad Peithmann

*Helmholtz Institute for Radiation and Nuclear Physics, University of Bonn, Nußallee 14-16, D-53115 Bonn, Germany*

Theo Woike

*Institute for Crystallography, University of Cologne, Zùlpicherstrasse 49b, D-50674 Cologne, Germany*

(Received 1 August 2007; revised manuscript received 5 March 2008; published 2 April 2008)

The average formal oxidation state of Cu in lithium niobate (LN) crystals doped with different copper levels (0.1–0.7 wt %), as well as in oxidized and reduced copper-doped LN crystals, is determined by x-ray and uv-visible and ir absorption spectroscopy and found to vary between  $1.2 \pm 0.2$  and  $1.8 \pm 0.2$ . The average formal oxidation state of Cu does not notably depend on the Cu concentration (for the range 0.1–0.3 wt %) upon simultaneous diffusion and oxidation of the doped crystals; but it does depend on the Cu concentration upon simultaneous reduction of the doped crystals. The x-ray absorption near-edge structure (XANES) and extended x-ray absorption fine structure analyses of the spectra measured at the Cu *K* edge provide evidence that all copper atoms are incorporated predominantly onto Li sites. Two distinct sites can be distinguished,  $\text{Cu}^{2+}$  and  $\text{Cu}^{1+}$  sites, coordinated sixfold and twofold by oxygen atoms, respectively. This result is supported by calculations of Cu *K* XANES spectra with the FEFF8.2 code. No experimental evidence is found for formation of metallic copper or copper oxide clusters in the LN crystals. One of the charge compensation mechanisms upon reduction of the LN crystals is outgassing of O atoms. Reduction of the Nb formal oxidation state is likely for total charge compensation. However, Nb *L*<sub>III</sub> XANES and ir absorption studies do not provide any evidence for this.

DOI: [10.1103/PhysRevB.77.144103](https://doi.org/10.1103/PhysRevB.77.144103)

PACS number(s): 77.84.Dy, 61.05.cj, 42.70.–a, 85.40.Ry

**I. INTRODUCTION**

The photorefractive properties of lithium niobate ( $\text{LiNbO}_3$ , LN) are widely employed in various applications, e.g., holographic data storage<sup>1,2</sup> and wavelength filters for telecommunication devices.<sup>3,4</sup> Significantly improved photorefractive properties are achieved by doping the LN crystals with transition metals like Fe,<sup>5–7</sup> or Cu ( $\text{LiNbO}_3:\text{Cu}$ ).<sup>8,9</sup> These metal atoms are found in two valence states  $\text{Cu}^{1+}$  and  $\text{Cu}^{2+}$  ( $\text{Fe}^{2+}$  and  $\text{Fe}^{3+}$ ), which act as sources ( $\text{Cu}^{1+}$  and  $\text{Fe}^{2+}$ ) and traps ( $\text{Cu}^{2+}$  and  $\text{Fe}^{3+}$ ) of electrons. Upon inhomogeneous illumination, electrons are excited into the conduction band, where they migrate due to drift, diffusion, and the bulk photovoltaic effect<sup>10</sup> and are finally trapped by the  $\text{Cu}^{2+}$  or  $\text{Fe}^{3+}$  impurity centers. The redistributed charge builds up space-charge fields, which modulate the refractive index via the electro-optic effect.<sup>11,12</sup>

It has been shown that highly concentrated copper doping in LN crystals causes a refractive index change ( $\Delta n$ ) comparable to that of less concentrated iron doping in LN crystals.<sup>13</sup> However, copper-doped crystals can be prepared by a cheaper and easier diffusion process,<sup>8,14</sup> as the diffusion constant of copper exceeds that of iron by a factor of 500.<sup>14,15</sup> An increase in  $\Delta n$ , the key factor in enhancing the storage capacity of a hologram,<sup>13</sup> is achieved by raising the content of  $\text{Cu}^{2+}$  traps in a LN crystal. However, at a high level of  $\text{Cu}^{2+}$  a decrease of  $\Delta n$  is observed.<sup>13</sup> In order to tune the photorefractive properties of the doped crystals, a detailed knowledge of the average valency of the copper atoms, as well as their local structure, e.g., site of occupation, is desirable.

The structure of LN consists of hexagonal close-packed oxide ions, where two-thirds of the face-sharing octahedral sites are occupied by cations, i.e., Li or Nb atoms, and one-third are empty. Due to electrostatic repulsions, the Li and Nb atoms are not in the middle of the octahedra, but shifted in opposite directions along the *z* axis.<sup>16</sup> In the congruently melting LN used in this study, around 6% of the Li atoms are missing.<sup>17</sup> The majority of the published studies on copper atoms incorporated into a LN matrix (prepared by a solid-state reaction<sup>18</sup> or an ion exchange method<sup>19</sup>) support the hypothesis that the doped Cu atoms predominantly occupy Li sites.<sup>18,19</sup> However, a detailed study of the electronic and geometrical structure upon systematic change in copper valence and concentration (0.1–0.7 wt % of Cu) is not yet available.

X-ray absorption spectroscopy (XAS) techniques, including x-ray absorption near-edge structure (XANES) and extended x-ray absorption fine structure (EXAFS) spectroscopy, probe the local electronic and geometrical environment of an element. They are particularly appropriate for characterizing doped materials with small dopant concentrations. There are numerous XANES studies demonstrating its ability to detect valence changes and to estimate the average formal oxidation state of a probed element; see, e.g., Ref. 20. XANES analysis is also a valuable tool for identifying occupation site symmetry. Detailed EXAFS analysis provides information on the local geometric structure around the probed element including and beyond the first coordination shell (up to  $\sim 6$  Å), without need of long-range order. Alternatively, the concentration and average formal oxidation state of copper are determined by means of absorption spectroscopy in

TABLE I. The concentrations of  $\text{Cu}^{1+}$  and  $\text{Cu}^{2+}$  ( $c_{\text{Cu}^{1+}}$  and  $c_{\text{Cu}^{2+}}$ ) and the total Cu concentration determined by uv-visible and ir absorption measurements ( $c_{\text{Cu}}$ ).

Notation for the samples and spectra	Cu-layer thickness (nm)	$c_{\text{Cu}^{1+}}$ ( $10^{24} \text{ m}^{-3}$ ) $\pm 15\%$	$c_{\text{Cu}^{2+}}$ ( $10^{24} \text{ m}^{-3}$ ) $\pm 15\%$	$c_{\text{Cu}}$ ( $10^{24} \text{ m}^{-3}/\text{wt } \%$ ) $\pm 15\%$
200_1	200	8	33	41/0.1
200_2	200	17	13	30/0.1
200_3	200	6	31	37/0.1
500_1	500	18	56	74/0.2
500_2	500	31	35	66/0.2
500_3	500	12	59	71/0.2
1000_1	1000	24	81	105/0.3
1000_2	1000	38	52	90/0.2
1000_3	1000	19	99	118/0.3
2000_1	2000	73	48	121/0.3
2000_1_a	2000	90	184	274/0.7
3000_2_a	3000	87	23	110/0.3

the ir and visible spectral regions. The reliability of this technique for studying the formal oxidation state of metals doped in LN crystals has been demonstrated in several publications (see, for example, Refs. 13 and 20).

The goals of our investigation are (i) to define the average formal oxidation state of Cu in indiffused, reduced, and oxidized LN crystals with different (0.1–0.7 wt % of Cu) doping levels of copper atoms, (ii) to identify not only the major site of incorporation (Li or Nb site) of the Cu atoms in all crystals, but also the structural differences between the  $\text{Cu}^{1+}$  and  $\text{Cu}^{2+}$  sites in the indiffused and reduced LN crystals, and, finally, (iii) to provide evidence for the charge compensation mechanisms during the reduction treatment.

## II. PREPARATION OF THE SAMPLES

The  $\text{LiNbO}_3:\text{Cu}$  samples were prepared from commercially available X-cut wafer material (thickness 1 mm). The wafers were cut into pieces of  $9 \times 10 \text{ mm}^2$ , where the 10 mm axis is parallel to the crystallographic  $c$  axis. After cutting, layers of copper were evaporated onto the surface in thicknesses ranging from 200 to 2000 nm. The samples were then annealed at 1000 °C for 24 h in air to allow Cu to diffuse into the crystal volume.<sup>8</sup> The samples 200\_1, 500\_1, and 1000\_1 were prepared in one single diffusion step. Sample 2000\_1\_a is first coated with 1000 nm Cu, annealed, coated for a second time, and subsequently annealed again. For comparison sample 2000\_1 was prepared in one single step using a 2000 nm layer.

After the diffusion process, samples were either oxidized in  $\text{O}_2$  atmosphere at 1000 °C for 5 h or reduced in vacuum about  $10^{-3}$  mbar for 5 h at 1000 °C. Thereby the concentration ratio  $c_{\text{Cu}^{2+}}/c_{\text{Cu}^{1+}}$  was changed. One sample, 3000\_2\_a, was diffused and reduced in a single step by annealing at 1000 °C in vacuum for 24 h. The 200, 500, and 1000 sample series were diffused, reduced, and oxidized at the same time.

The notation for all studied LN crystals and the XANES spectra are listed in Table I. The three-digit number in the notation indicates the thickness of the copper layer in nanometers, e.g., 200 nm. The numbers from 1 to 3 specify the presence or lack of subsequent treatment of the crystal: \_1 indicates indiffused, \_2 reduced, and \_3 oxidized. The letter \_a shows a two-step diffusion process for the 2000\_1\_a sample and simultaneous diffusion and reduction of the crystal for the 3000\_2\_a sample.

## III. EXPERIMENT, METHODS, AND DATA EVALUATION

XAS experiments were performed at the INE beamline at the ANKA 2.5 GeV synchrotron radiation facility, Karlsruhe, Germany. For details about the instrumentation at this beamline, see Ref. 21. A Lemonnier-type<sup>22</sup> double-crystal monochromator equipped with a set of Ge(422) (Cu  $K$  edge) or Si(111) (Nb  $L_{\text{III}}$  edge) crystals was employed for energy monochromatization. For energy calibration of Cu  $K$  edge spectra a photon energy of 8979 eV was set to the first inflection point of the  $K$  edge spectrum of a copper foil, simultaneously measured with the samples and references. The Nb  $L_{\text{III}}$  edge spectra were energy calibrated against the sulfur  $K$  edge white line (WL) (the first intense absorption resonance of the spectrum) of  $\text{ZnSO}_4$  set to 2481.44 eV. The copper-doped LN crystals were ground, and absorption spectra of the powder samples were taken at the Cu  $K$  edge (8979 eV) in fluorescence mode and at the Nb  $L_{\text{III}}$  edge (2371 eV) in transmission mode. For the measurements in fluorescence mode, a five-element Ge solid state detector (Canberra type) was used. During the measurements in fluorescence mode, each sample was positioned on a goniometer; it was rotated  $0.001^\circ$  with respect to the primary beam after each spectrum, in order to average out possible diffraction peaks. The spectra of the references Cu,  $\text{Cu}_2\text{O}$ , and CuO were measured in transmission mode.

All Cu  $K$  XANES spectra were measured in the energy interval from 8930 to 9130 eV, with 0.5 eV step width and

2 s integration time. At the Nb  $L_{III}$  edge, the XANES spectra were measured in the energy interval from 2324 to 2360 eV, with 0.1 eV step width and 2 s integration time. At least five XAS (XANES+EXAFS) spectra were collected from each sample measured in fluorescence mode, in order to check for reproducibility of the spectral features and to improve the statistics. XANES data reduction consisted of subtraction of a linear background fitted to the pre-edge region, from 8829 to 8959 eV for Cu  $K$  edge spectra and from 2324 to 2360 eV for Nb  $L_{III}$  edge spectra, followed by normalization of the spectra to an edge jump of 1 at 9121 (Cu) or 2439 eV (Nb).

The ARTEMIS program package<sup>23</sup> was used for EXAFS analyses. The XAFS signal [ $\chi(k)$ ] measured at the Cu  $K$  edge, covering a  $k$  range from 2.3 to 10  $\text{\AA}^{-1}$ , was Fourier transformed to  $R$  space using  $k$  weightings of 1, 2, and 3 and a Hanning window with window sills  $dk$  equal to 2. The ARTEMIS option for simultaneous fits with all three  $k$  weightings (1, 2, and 3) was used. The fit was performed in  $R$  space over a range from 1 to 3.1  $\text{\AA}$  for the 200, 500, and 1000 sample series and from 1 to 3.7  $\text{\AA}$  for the 2000 and 3000 sample sets. For the initial model the structure of  $\text{LiNbO}_3$  (ICSD 28294) was used. The amplitude reduction factor was held constant to 0.85 ( $S_0^2$ ), the value obtained from initial fits for a Cu foil Fourier-transformed (FT) EXAFS spectrum measured under the same experimental conditions. The error range of the  $S_0^2$  is estimated to be  $\pm 0.04$ .

During fits of the FT EXAFS spectra, the  $E_0$  and the Debye-Waller factors were varied. The first coordination shell (Cu-O) was first fitted using a defined coordination number, according to the model, and with varying distance. The fit was repeated with fixed distance and varying coordination number to ascertain if this led to reduction of the coordination number. This was the case for the reduced crystals. Therefore, the distance and coordination number were consecutively fixed and varied until the best fit was obtained. In the next step the coordination number and distance for the first coordination shell were held constant at their best-fit values and the fit range was extended to 3.1 or 3.7  $\text{\AA}$ . The fit procedure was repeated using the first single-scattering paths with the highest amplitude contribution, i.e., Cu-Nb, in this distance range. During the fit procedure, care was taken that the number of varying parameters was always half or less the number of independent data points  $N_{\text{ind}}$ ,<sup>34,35</sup> defined as

$$N_{\text{ind}} = \frac{2(k_{\text{max}} - k_{\text{min}})(R_{\text{max}} - R_{\text{min}})}{\pi}$$

For all performed fits, the obtained  $r$  factor (overall goodness of fit) was 0.01 or smaller, which means that data and fit agree on average within 1% or better.

The best-fit values for our set of parameters (variables) were found by minimizing  $\chi^2$  by applying the Levenberg-Marquardt method.<sup>34</sup>  $\chi^2$  is defined as

$$\chi^2 = \sum_{i=1}^{N_{\text{ind}}} \left( \frac{-f_i}{\epsilon_i} \right)^2,$$

where  $f_i$  is the function to minimize (the difference between data and model), and  $\epsilon_i$  is the uncertainty in the function to minimize. The Levenberg-Marquardt algorithm is imple-

mented in the FEFFIT fit program,<sup>35</sup> which is part of the ARTEMIS program package. The uncertainties of the parameter fit values are estimated as the value by which  $\chi^2$  will change to a value less than  $\chi^2 + 1$ . Here, it should be noted that the uncertainties are rescaled by  $\sqrt{\chi_0^2}$ .  $\chi_0^2$  is the reduced  $\chi^2$  equal to  $\chi^2/\nu$ .  $\nu = N_{\text{ind}} - N_{\text{vars}}$  is the number of degrees of freedom in the fit, where  $N_{\text{vars}}$  is the number of variables in the fit.

We attempted to simulate the Cu  $K$  XANES spectra of the 3000\_2\_a and 200\_1 samples using the FEFF8.2 code.<sup>24</sup> The purpose of the calculations was to check whether it is possible to reproduce the Cu  $K$  XANES spectra using the results from the EXAFS analyses as input. The calculations were done for a cluster of 230 atoms and no experimental broadening was taken into account. In the FEFF 8.2 calculations the EXCHANGE, SCF, FMS, and XANES cards were used. The Hedin-Lundqvist self-energy was chosen as exchange-correlation potential, which is the default setting of the EXCHANGE card. We did the calculations using a modified structural model with Cu incorporated into the Li site in two ways, either by substituting only the absorbing Li atom by a Cu atom or by substituting 100% of the Li atoms by Cu atoms. As the obtained spectra are very similar, only the first calculations (substitution of the absorbing Li atom by a Cu atom) are shown in Sec. IV C. The atomic cluster employed in the calculation was modified, in order to approximately reflect the distances and coordination numbers obtained from the EXAFS analysis.

The modifications for simulating the 200\_1 and 3000\_2\_a spectra are as follows. (1) To simulate the 200\_1 experimental spectrum, O and Li atoms were initially moved  $-0.2 \text{ \AA}$  (if the  $z$  coordinate is positive) or  $+0.2 \text{ \AA}$  (if the  $z$  coordinate is negative) along the  $z$  axis; the Li atoms and the absorbing Cu atom with  $z$  coordinates equal to zero were not moved. For a second simulation step Nb atoms were shifted  $+0.1 \text{ \AA}$  (if the  $x$  coordinate is positive) or  $-0.1 \text{ \AA}$  (if the  $x$  coordinate is negative) along the  $x$  axis. The cluster was then modified by shifting the central absorbing Cu atom  $+0.16 \text{ \AA}$  along the  $z$  axis, the three oxygen atoms from the first shell with negative  $z$  coordinates  $+0.5 \text{ \AA}$  along the  $z$  axis, and the remaining three first-shell O atoms  $-0.05 \text{ \AA}$  along the  $z$  axis. In a final step, the coordinates of the four niobium atoms closest to the absorbing copper atom were refined in the simulation until close agreement with the Cu-Nb1 and Cu-Nb2 distances obtained from the EXAFS analysis was achieved. (2) The modifications of the atomic cluster used for simulation of the 3000\_2\_a spectrum included removing three O atoms with positive  $z$  coordinates and one O atom with negative  $z$  coordinate from the first coordination shell from the list of atomic cluster coordinates. The two remaining O atoms in the absorber Cu first coordination shell were then shifted by  $+0.2 \text{ \AA}$  along the  $z$  axis. The coordinates of the four Nb atoms closest to the absorbing Cu atom were changed by shifting the Nb1 atom  $+0.1 \text{ \AA}$  along the  $z$  axis, the two Nb2 atoms with negative  $x$  coordinates  $-0.2 \text{ \AA}$  along the  $x$  axis, and the one Nb2 atom with a positive  $x$  coordinate  $+0.1 \text{ \AA}$  along the  $x$  axis.

Copper has two characteristic absorption bands in the uv-visible and ir spectra of  $\text{LiNbO}_3:\text{Cu}$ . Copper in the valence state  $\text{Cu}^{1+}$  shows a band in the uv-visible spectral range at

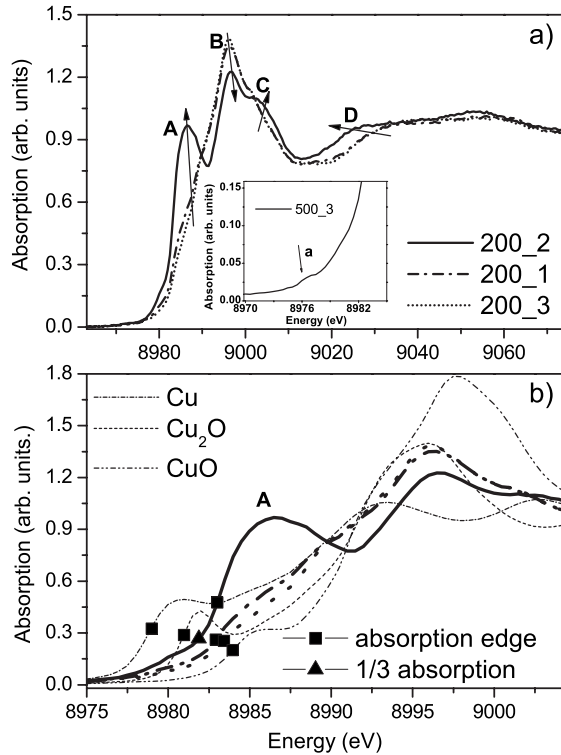


FIG. 1. Cu  $K$  XANES experimental spectra of the (a) 200\_1, 200\_2, and 200\_3 samples; (b) compared to Cu,  $\text{Cu}_2\text{O}$ , and CuO references over a smaller energy range. Inset: the preedge region of the Cu  $K$  XANES experimental spectrum of the 500\_3 sample.

385 nm, whereas  $\text{Cu}^{2+}$  exhibits a band in the ir at 1040 nm.<sup>8,12</sup> By measuring the corresponding absorption coefficients,  $\text{Cu}^{1+}$  and  $\text{Cu}^{2+}$  concentrations and hence the average formal oxidation state of Cu can be determined.

## IV. RESULTS AND DISCUSSION

### A. Average formal oxidation state of Cu

In Fig. 1(b), the three spectra of the 200 sample series are plotted along with Cu,  $\text{Cu}_2\text{O}$ , and CuO reference spectra. The energy positions of the series spectra are located between the  $\text{Cu}^{1+}$  and  $\text{Cu}^{2+}$  references, indicating a mixed valence state ( $\text{Cu}^{1+}$  and  $\text{Cu}^{2+}$ ) of the copper atoms in the samples. The energy of the 200\_2 spectrum lies closer to the  $\text{Cu}_2\text{O}$  reference spectrum, suggesting its having a higher valence than  $\text{Cu}^{1+}$ . The trends in the three spectra in Fig. 1(a) also indicate a shift in copper oxidation state toward higher average valence on going from the 200\_2 to the 200\_1 to the 200\_3 samples. The A and C resonances increase as B decreases, and resonance D shifts toward lower energies with reduction of the formal copper valency. The minor changes in the 200\_3 spectrum compared to the 200\_1 spectrum may indicate that the 200\_1 sample is already considerably oxidized during the diffusion process performed in air.

One way to quantitatively elucidate the formal valence of a metal oxide is to determine the energy position of the absorption edges in comparison with suitable reference compounds. These positions can be defined, for example, as the

TABLE II. Formal oxidation state of Cu for all studied samples determined by x-ray and ir-visible (ir-vis) absorption spectroscopy.

Sample	X-ray results	ir-vis results	Averaged value from the two methods
	$\pm 0.2$	$\pm 0.2$	$\pm 0.2$
200_1	1.7	1.8	1.8
200_2	1.2	1.4	1.3
200_3	1.8	1.8	1.8
500_1	1.7	1.8	1.8
500_2	1.4	1.5	1.5
500_3	1.8	1.8	1.8
1000_1	1.7	1.8	1.8
1000_2	1.4	1.6	1.5
1000_3	1.8	1.8	1.8
2000_1_a	1.7	1.7	1.7
2000_1	1.4	1.4	1.4
3000_2_a	1.2	1.2	1.2

first inflection points of the respective spectra, i.e., the maximum of the first intense peak in the first-derivative spectrum. However, this widely applied approach is not valid for the spectra of the reduced samples as they exhibit structures on the rising edge of their XANES. For example, the energy positions of the first inflection points of the 200\_1 and 200\_2 spectra almost coincide; whereas the 200\_3 spectrum is distinctly shifted toward lower energies [see Fig. 1(b)]. We therefore define the absorption edge energy as the energy point at 1/3 of the absorption level of the normalized spectra [an example is displayed in Fig. 1(b)]. Similar approaches for defining absorption edges are found in the literature, e.g., the energy position of the maximum of a resonance on the absorption edge<sup>25</sup> or from the WL is used.<sup>26</sup> A linear model was employed to fit the edge energy position of the reference spectra of Cu,  $\text{Cu}_2\text{O}$ , and CuO as a function of copper valence 0, +1, and +2 formal oxidation states, respectively. This linear function was used as a calibration line to determine the average formal oxidation states of all samples; a graphical example of the empirical method can be seen in Ref. 20. Within the error bars, the obtained values (Table II) are in agreement with the values obtained from the absorption measurements in the infrared and visible spectral ranges.

The 500\_1 and 1000\_1 Cu  $K$  XANES spectra (not shown) resemble the 200\_1 spectrum. There is no qualitative or quantitative evidence for changes in copper average valence in these three samples; the average valence of copper is  $1.8 \pm 0.2$  in all three (see Table II). Since the crystals are diffused simultaneously, this finding shows that the average formal oxidation state of copper does not depend on the copper concentration within the concentration range studied (0.1–0.3 wt % of Cu). The average formal copper valence is also the same for the three oxidized crystals, as the 500\_3 and 1000\_3 spectra (not shown) are identical to the 200\_3 spectrum (Fig. 1). However, pronounced differences are present in the spectra of the simultaneously reduced samples, shown in Fig. 2. Analogous trends in spectral changes in the features A, B, C, and D (Fig. 2) discussed above are observed

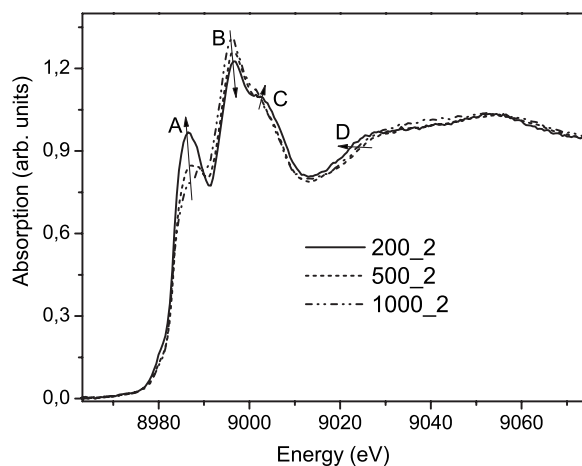


FIG. 2. Experimental Cu K XANES for the 200\_2, 500\_2, and 1000\_2 samples.

here as a function of decreasing copper concentration. This indicates an increase in the relative amount of  $\text{Cu}^{1+}$  in the order 1000\_2, 500\_2, 200\_2.

The average copper valence differs in the 2000\_1\_a, 2000\_1, and 3000\_2 crystals (Table II), i.e., it is  $1.7 \pm 0.2$  for the 2000\_1\_a sample,  $1.4 \pm 0.2$  for the 2000\_1 sample, and  $1.2 \pm 0.2$  for the 3000\_2\_a sample. The Cu K XANES spectra of the three samples are displayed in Fig. 3. The resonance A, which increases with increasing contribution of  $\text{Cu}^{1+}$  (Fig. 3, Table II), is observed in the 2000\_1 and the 3000\_2\_a spectra. Clearly, it is possible to reach a desirable average Cu valency and high doping level of copper (0.3–0.7 wt % of Cu) by applying simultaneous or subsequent diffusion and annealing procedures. The Cu K XANES spectra (Fig. 3) resemble the spectra of the LN crystals with low copper concentration, which suggests that there are no major electronic or geometrical structural differences in the highly doped crystals. However, the Cu atoms in the 2000\_1 crystal are already considerably reduced during the indiffusion process, i.e., no additional reduction treatment is performed.

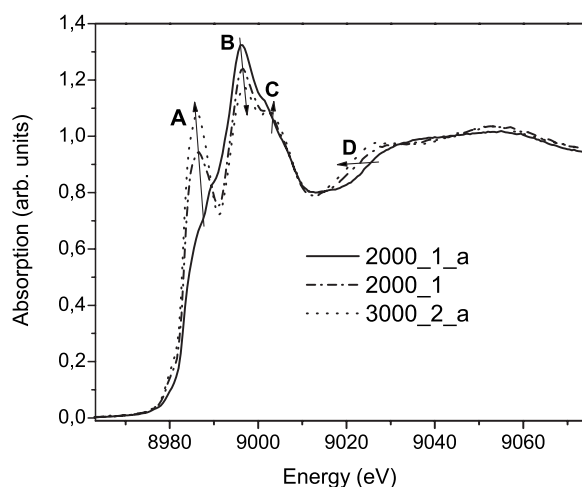


FIG. 3. Experimental Cu K XANES for the 2000\_1\_a, 2000\_1, and 3000\_2\_a samples.

Further experiments should be performed to study the influence of high Cu concentrations on the  $\text{Cu}^{2+}:\text{Cu}^{1+}$  ratio.

### B. Local atomic environment of the Cu atoms

Figures 4 and 5 depict the EXAFS spectra (in  $R$ ,  $q$ , and  $k$  space) of all studied LN crystals. The fit results (Table III) allow us to conclude that the Cu atoms occupy the Li site. Three Nb atoms are found at about 3.1 Å distance, varying from 3.04 to 3.15 Å from the indiffused to the reduced crystals. The model of Cu on the Li site implies three Nb atoms at 3.06 Å. The high scattering amplitude of the heavy Nb atoms leads to a pronounced peak A at around 3 Å. If Cu were located at Nb sites, backscattering from the lighter Li atoms at this distance would result in a significantly less pronounced feature. Moreover, the fingerprint for a Cu on Nb site model, i.e., a distinct peak due to the Nb-Nb coordination at around 3.5 Å, is not present in the experimental spectra (see Figs. 4 and 5), also indicating that Cu does not occupy Nb sites.

In principle, the FT peak A (Figs. 4 and 5) might also be caused by scattering of the photoelectron on other heavy metal atoms, i.e., in our case other Cu atoms. Thus, we have assumed and tested two more models: incorporation of Cu into Li and Nb sites and formation of a copper oxide phase embedded within the  $\text{LiNbO}_3$  matrix. In both cases, the quality of the fits using those models was poor, which gives us confidence in ruling them out. Please note that this excludes the presence of Cu-O-Cu coordination in copper-doped LN crystals.

After diffusion of Cu atoms, about  $20\% \pm 15\%$   $\text{Cu}^{1+}$  and  $80\% \pm 15\%$   $\text{Cu}^{2+}$  are found in the crystals (Table I). After reduction of the doped crystals, the amounts are converted to about  $80\% \pm 15\%$   $\text{Cu}^{1+}$  and  $20\% \pm 15\%$   $\text{Cu}^{2+}$  (Table I). Our results support strongly the hypothesis that there is just one site for all Cu atoms, independent of their formal valence, namely, the Li site. It is now important to identify the changes in the local geometry that are connected with valency changes due to oxidation and reduction.

Changes in the local coordination geometry upon changes in formal oxidation state are reflected in the reduced number of O atoms in the first coordination shell in the samples with average formal valence of Cu equal to or lower than  $1.5 \pm 0.2$  (Figs. 4 and 5, Table III). The effect is most significant for the 200\_2, 2000\_1, and 3000\_2\_a samples, showing a decrease in average coordination number from six to around three O atoms. Changes in coordination symmetry with copper valence are also observed in the XANES spectra. The weak preedge peak at around 8978 eV (inset in Fig. 1) is not present in XANES spectra of compounds containing  $\text{Cu}^{1+}$  because of the completely filled Cu 3d shell. The preedge peak is assigned to a 1s-3d transition in the case of CuO by Bocharov *et al.*<sup>33</sup> However, in compounds without inversion symmetry, this feature can also be due to transition of the 1s electron to a molecular orbital, formed by hybridization of the O 2p and Cu 3d orbitals. The existence of the preedge peak can serve as a fingerprint for a high contribution of  $\text{Cu}^{2+}$ , and its energy position can serve as a fingerprint for site symmetry of the  $\text{Cu}^{2+}$  atoms.<sup>27–29</sup> This feature is

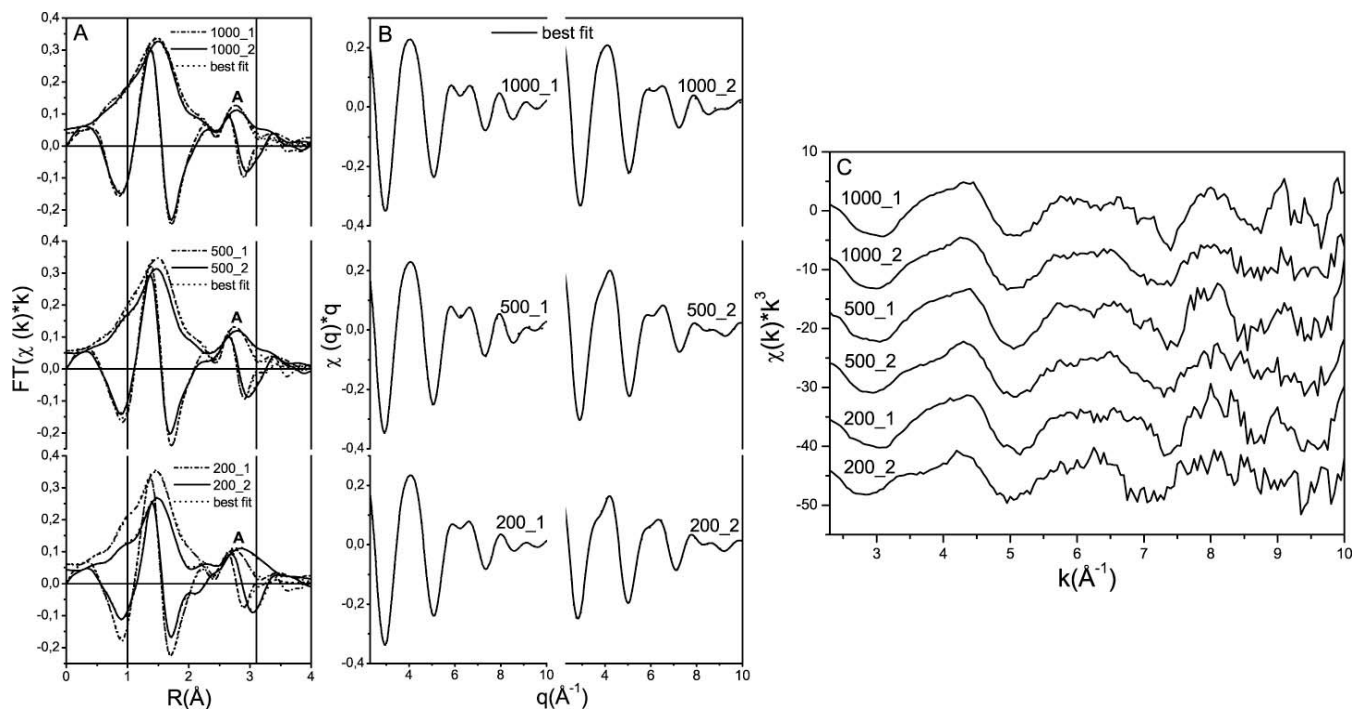


FIG. 4. EXAFS spectra in  $R$  (amplitude and imaginary parts of the FT EXAFS spectra) (a),  $q$  (b), and  $k$  (c) space and their best fits for the 200\_2, 200\_1, 500\_2, 500\_1, 1000\_2, and 1000\_1 samples.

also detectable in the first derivative of a spectrum. Figure 6 displays the preedge region of the first-derivative XANES spectra of all studied samples and references. The preedge peaks show up as maxima and are indicated with a line and arrows in the figure. The energy position of the XANES preedge peaks of the 200\_3, 500\_3, 1000\_1, 1000\_3, and 2000\_1\_a samples coincides with that of the octahedral compound. This feature, in contrast, is shifted by 1 eV to higher energies for the square planar compound CuO (Fig. 6). This suggests predominant octahedral site symmetry of the  $\text{Cu}^{2+}$  atoms in these samples. The coordination numbers obtained

from the EXAFS analysis also suggest octahedral site symmetry of the Cu atoms in the crystals with formal valence equal to or higher than  $1.7 \pm 0.2$ .

We therefore can use the 200\_1, 500\_1, and 1000\_1 Cu  $K$  XANES spectra as a sort of reference containing mainly  $\text{Cu}^{2+}$  in an octahedral geometry and the 3000\_2\_a Cu  $K$  XANES spectrum as a reference containing mainly  $\text{Cu}^{1+}$ . Linear combination least-squares fits of the 200\_2, 500\_2, 1000\_2, and 2000\_1 spectra were performed using the 200\_1 and 3000\_2\_a spectra as  $\text{Cu}^{2+}$  and  $\text{Cu}^{1+}$  reference compounds. The aim was to verify whether  $\text{Cu}^{2+}$  atoms in an

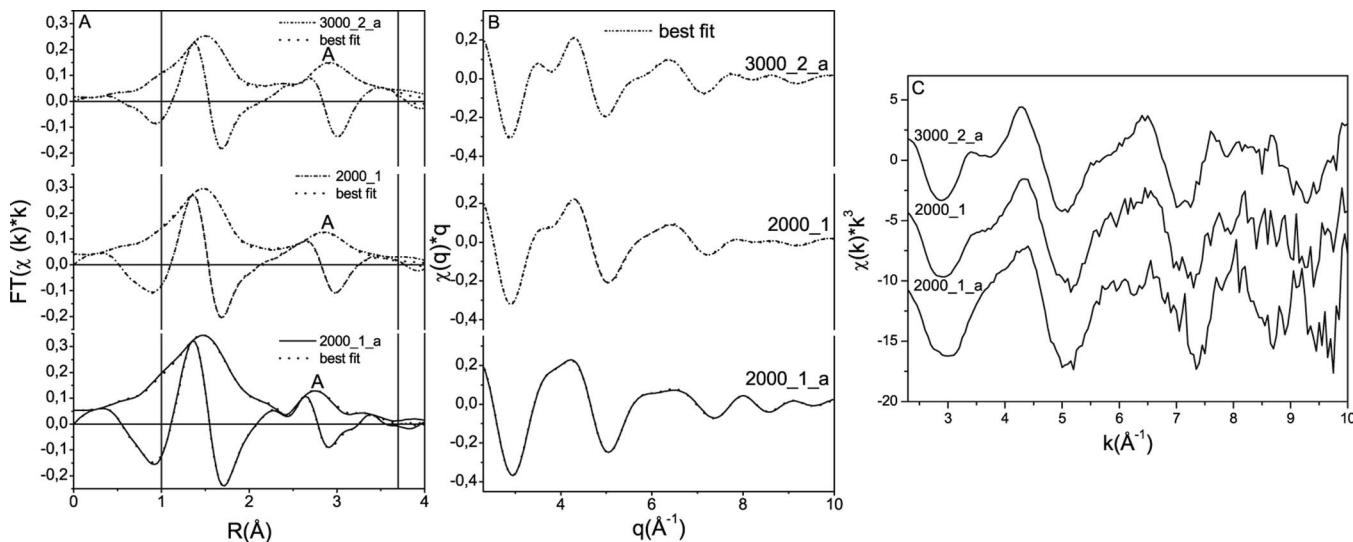


FIG. 5. EXAFS spectra in  $R$  (amplitude and imaginary parts of the FT EXAFS spectra) (a),  $q$  (b), and  $k$  (c) space and their best fits for the 2000\_1\_a, 2000\_1, and 3000\_2\_a samples.

TABLE III. Results of the EXAFS analyses. The type of atom neighboring the absorbing Cu atom is given in the first column. The structural parameters and the employed model are in the remaining columns:  $N$ , coordination number;  $R$  (Å), distance;  $N_m$ , coordination number of the Cu in Li site model;  $R-R_m$  (Å), difference between fitted and model distance;  $\sigma^2$  (Å<sup>2</sup>), Debye-Waller factor.

	$N$	$N_m$	$R$ (Å) $\pm 0.01$	$R-R_m$ (Å)	$\sigma^2$ (Å <sup>2</sup> ) $\pm 0.001$	$N$	$N_m$	$R$ (Å) $\pm 0.01$	$R-R_m$ (Å)	$\sigma^2$ (Å <sup>2</sup> ) $\pm 0.001$	$N$	$N_m$	$R$ (Å) $\pm 0.01$	$R-R_m$ (Å)	$\sigma^2$ (Å <sup>2</sup> ) $\pm 0.001$
	200_1					500_1					1000_1				
O1	6.0	3.0	1.98	-0.08	0.012	6.0	3.0	2.00	-0.07	0.012	6.0	3.0	2.00	-0.06	0.013
O2		3.0					3.0					3.0			
Nb1	1.0	1.0	2.99	-0.02	0.012 <sup>a</sup>	1.0	1.0	3.01	0.00	0.010	1.0	1.0	3.02	0.01	0.010
Nb2	3.0	3.0	3.04	-0.02	0.012 <sup>a</sup>	3.0	3.0	3.05	0.00	0.010	3.0	3.0	3.06	0.01	0.010
O3	3.0	3.0	3.22	-0.06	0.012	3.0	3.0	3.22	-0.06	0.012	3.0	3.0	3.24	-0.05	0.013
	200_2					500_2					1000_2				
O1	3.4 ± 0.4	3.0	2.01	-0.06	0.005	4.4 ± 0.2	3.0	1.99	-0.07	0.007	5.5 ± 0.5	3.0	2.01	-0.05	0.012
O2		3.0				1.1 ± 0.3	3.0	2.25	0.01	0.007		3.0			
Nb1	1.0	1.0	3.09	0.08	0.007	1.0	1.0	3.09	0.08	0.019 <sup>a</sup>	1.0	1.0	3.03	0.02	0.012 <sup>a</sup>
Nb2	3.0	3.0	3.14	0.08	0.007	3.0	3.0	3.14	0.09	0.019 <sup>a</sup>	3.0	3.0	3.07	0.02	0.012 <sup>a</sup>
O3	1.7 ± 0.7	3.0	3.14	-0.14	0.005	3.0	3.0	3.21	-0.07	0.007	2.3 ± 0.8	3.0	3.15	-0.13	0.012
Nb3	3.0	3.0	3.30	-0.08	0.007										
	2000_1_a					2000_1					3000_2_a				
O1	6.0	3.0	1.99	-0.07	0.012	4.2 ± 0.3	3.0	1.99	-0.08	0.008	3.3 ± 0.2	3.0	2.00	-0.06	0.006
O2		3.0					3.0					3.0			
Nb1	1.0	1.0	3.01	0.00	0.011	1.0	1.0	3.08	0.07	0.016	1.0	1.0	3.10	0.09	0.007
Nb2	3.0	3.0	3.06	0.00	0.011	3.0	3.0	3.13	0.08	0.016	3.0	3.0	3.15	0.10	0.007
O3	3.0	3.0	3.21	-0.08	0.012	3.2 ± 0.4	3.0	3.16	-0.12	0.008	2.0 ± 0.4	3.0	3.24	-0.05	0.006
Nb3	3.0	3.0	3.72	0.30	0.011	3	3.0	3.21	-0.17	0.016	3.0	3.0	3.29	-0.08	0.007
O5											0.7 ± 0.2	3.0	4.06	0.13	0.006

<sup>a</sup>The error bar is  $\pm 0.002$ .

octahedral geometry contribute to the samples with formal valence equal to or higher than  $1.5 \pm 0.2$ . An example from these analyses is shown in Fig. 7. The linear combination of 30% of the 200\_1 spectrum and 70% of the 3000\_2\_a spectrum is plotted along with the 2000\_1 spectrum. The good agreement between simulated and experimental spectra and the finding that Cu<sup>2+</sup> and Cu<sup>1+</sup> atoms contribute about  $40\% \pm 15\%$  and  $60\% \pm 15\%$ , respectively, in the 2000\_1 sample suggest that the Cu<sup>2+</sup> atoms in the 2000\_1 sample are mainly sixfold coordinated by O atoms and the Cu<sup>1+</sup> atoms are mainly twofold coordinated by O atoms; four O atoms on average in the first coordination shell are found by the EXAFS analysis for this sample. This result is valid for all reduced crystals, as it was possible to simulate their spectra with a linear combination of the 200\_1 and 3000\_2\_a spectra (200\_2, 30% 200\_1+70% 3000\_2\_a; 500\_2, 50% 200\_1+50% 3000\_2\_a; 1000\_2, 60% 200\_1+40% 3000\_2\_a).

The resonance A [Fig. 1(a)] is assigned to the transition of the 1s electron to the doubly degenerate  $4p_{x,y}$  state.<sup>27</sup> In their systematic XAS study of 19 Cu<sup>1+</sup>- and 40 Cu<sup>2+</sup>-containing compounds, Kau *et al.* showed that resonance in Cu *K* XANES between 8983.5 and 8984.5 eV with an intensity

comparable to the intensity of the WL of a conventionally normalized XANES spectrum appears in Cu *K* XANES spectra of twofold-coordinated Cu<sup>1+</sup> compounds.<sup>27</sup> The presence of resonance A, which resembles that described by Kau *et al.* (Figs. 1–3) in the Cu *K* XANES spectra of the reduced LN crystals, confirms the EXAFS result that the major part of the Cu<sup>1+</sup> atoms in these crystals are twofold coordinated. The resonance is most intense in the Cu *K* XANES spectra of the crystals with highest Cu<sup>1+</sup> contribution (e.g., sample 3000\_2\_a with average copper valence 1.2).

In order to compare the Cu-O bond lengths for the crystals with formal valence of Cu  $\leq 1.5 \pm 0.2$  and  $\geq 1.7 \pm 0.2$ , several factors should be considered. A bond length is influenced by the formal valence of the absorbing atom, electronegativity of the ligands, and the local coordination symmetry. A metal-oxygen bond distance increases with a decrease in the formal oxidation state of the metal; see, e.g., Ref. 30. This trend is valid for the Cu-O bond distance in the Cu<sup>1+</sup>-containing compounds Cu<sub>2</sub>O (1.85 Å, ICSD 63281) compared to the Cu-O distance in the Cu<sup>2+</sup> compound CuO (1.69 Å, ICSD 67850). Site symmetry also has a significant influence on the metal-oxygen bond length. The Cu<sup>2+</sup> com-

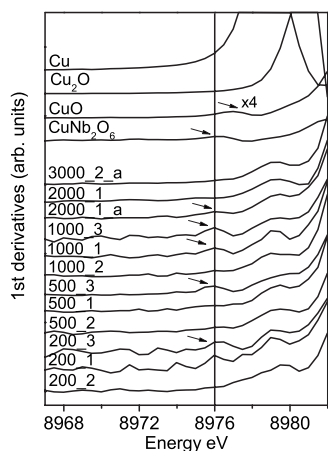


FIG. 6. First derivative of the experimental Cu K XANES spectra of all studied samples and Cu, Cu<sub>2</sub>O, CuO, and CuNb<sub>2</sub>O<sub>6</sub> references.

pound CuNb<sub>2</sub>O<sub>6</sub>, which has Cu in octahedral coordination, has a Cu-O bond length (1.97 Å, ICSD 74424) 0.12 Å longer than CuO with square planar coordination. Such a symmetry variation could explain the almost the same Cu-O distance difference for the indiffused and reduced samples obtained from the EXAFS analysis.

The obtained  $\sigma_{\text{Cu-O}}^2$  parameters (Table III) for the crystals with average formal oxidation state of Cu  $\geq 1.7$  are comparable to values obtained from a temperature-dependent EXAFS study of copper-doped magnesium oxides.<sup>36</sup> We consider this material an appropriate model system, because the nearly perfect octahedral oxygen coordination of the Cu<sup>2+</sup> ions at room temperature distorts at higher temperatures. Moreover, the Cu<sup>2+</sup> (0.73 Å) and Mg<sup>2+</sup> (0.72 Å) ions have almost the same ionic radii,<sup>37</sup> which explains the result that the substitution of Mg by Cu does not lead to significant structural distortion.<sup>36</sup> The  $\sigma_{\text{Cu-O}}^2$  parameters in Ref. 36 vary from 0.012 Å<sup>2</sup> (300 K) to 0.024 Å<sup>2</sup> (1500 K). Comparison of these values to the  $\sigma_{\text{Cu-O}}^2$  values obtained for our copper-doped LN crystals (0.006–0.013 Å<sup>2</sup>) indicate that our crys-

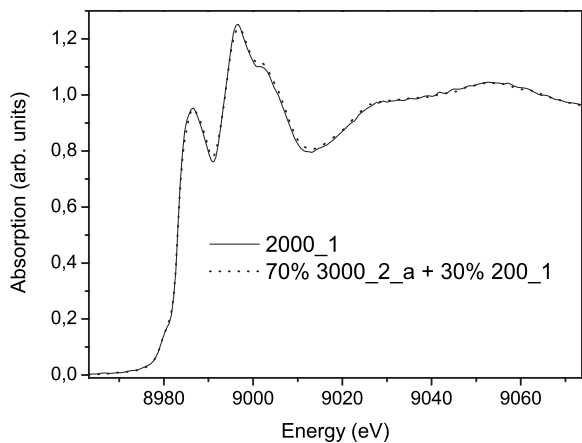


FIG. 7. Experimental Cu K XANES spectra for the 2000\_1 sample and the result of a linear combination least-squares fit using 70% 3000\_2\_a XANES and 30% 200\_1 XANES.

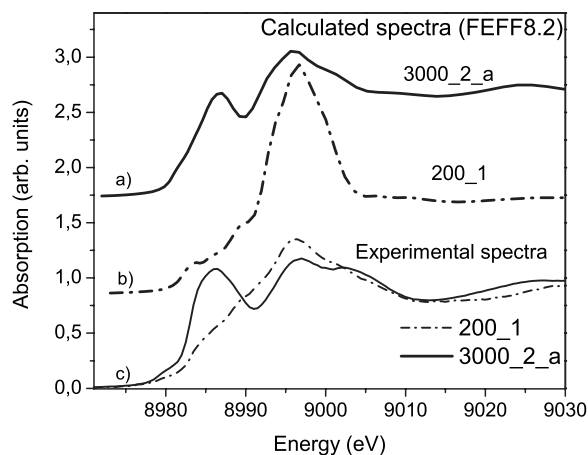


FIG. 8. Simulated (a) 3000\_2\_a and (b) 200\_1 Cu K XANES spectra and (c) experimental 200\_1 and 3000\_2\_a Cu K XANES spectra.

tals have undistorted sixfold-coordinated Cu<sup>2+</sup>. The reduced distortion of the octahedral Li site compared to undoped LN can be explained by the differing ionic radii of Li<sup>1+</sup> (0.63 Å, sixfold coordination) and Cu<sup>2+</sup> (0.73 Å, sixfold coordination).<sup>37</sup>

In contrast to the near-invariant Cu-O bond distance, the Cu-Nb distance is affected by the reduced formal valency and average oxygen coordination of the Cu atoms. The Cu-Nb distance increases with increasing copper reduction. For example, the 200\_1 sample has a Cu-Nb2 distance of  $3.04 \pm 0.01$  Å, whereas this distance in the 200\_2 sample is  $3.14 \pm 0.01$  Å (see Table III). This result suggests that the incorporated Cu atoms cause local structural disorders, i.e., local changes in the crystallographic parameters of the LiNbO<sub>3</sub> crystal. Formation of crystalline phases, other than LiNbO<sub>3</sub> is reported by x-ray diffraction studies on LN crystals doped with copper by an ion exchange method.<sup>19</sup> However, copper is inhomogeneously distributed in the sample studied in Ref. 19, whereas it is not the case for the copper-doped LN crystals studied here. See Ref. 7 for an example of a typical copper distribution profile.

### C. Simulation of the Cu K XANES spectra

In Fig. 8, the experimental and theoretical Cu K XANES spectra calculated with the FEFF8.2 code<sup>24</sup> for the 3000\_2\_a and 200\_1 samples are shown. These samples are selected as they are representatives of the two copper coordination symmetries, twofold-coordinated Cu<sup>1+</sup> and sixfold-coordinated Cu<sup>2+</sup>. In our simulation approach the atom coordinates of the atomic cluster used in the calculations were modified in order to reproduce values obtained from the EXAFS analysis for distances, within the error bars up to  $\sim 3$  Å, and coordination numbers. For simulation of the 200\_1 spectrum, the distances used are Cu-O=1.98 Å, Cu-Nb1=3.0 Å, and Cu-Nb2=3.04 Å. For simulation of the 3000\_2\_a spectrum, the distances are Cu-O=2.01 Å, Cu-Nb1=3.11 Å, and Cu-Nb2=3.16 Å. It was not sufficient to modify only the coordinates of the atoms of the first two shells for the 200\_1

spectrum (see Sec. III). Therefore, additional refinements of atomic coordinates of the distant atoms were done until close agreement between the experimental and simulated spectra was achieved. A similar approach for reproduction of an experimental XANES spectrum is followed by using the MXAN package.<sup>31,32</sup> In this package the initial atomic coordinates of a model compound with known structure are refined and a XANES spectrum is repeatedly calculated until the experimental and theoretical spectra closely agree. The refined distances between the absorber and the closest neighboring atoms are compared to those obtained from EXAFS analysis and x-ray diffraction.<sup>32</sup>

There is at least one configuration of atomic coordinates leading to satisfactory agreement between calculated and experimental spectra of the 200\_1 and 3000\_2\_a samples that accounts for the EXAFS results. Refined atomic coordinates from the XANES simulations support the hypothesis of the existence of two different Cu sites, i.e., twofold and sixfold coordinated by O atoms, in the samples with formal valence of Cu equal to or lower than  $1.5 \pm 0.2$ . The calculations demonstrate the utility of a top-down approach refining atomic coordinates by using EXAFS results as initial input to obtain good agreement between experimental and calculated spectra.

#### D. Charge compensation mechanism

The average number of oxygen ions next to Cu is reduced from six to three upon reduction of the doped LN crystals (Table III). This finding suggests that one of the mechanisms providing charge compensation upon reduction of the doped crystals is the outgassing of O atoms. In principle, the reduction treatment might lead not only to a lower formal valence of copper, but also to a change in the formal oxidation state of the Nb atoms, i.e., from an initial 5+ formal valence to a lower one. In order to identify Nb valence changes, the Nb  $L_{III}$  XANES spectra of the copper-doped LN have been recorded. The spectra for samples 1000\_1 and 1000\_2 are shown in Fig. 9 as examples and compared to spectra for  $\text{LiNbO}_3$  ( $\text{Li}^{1+}$ ,  $\text{Nb}^{5+}$ ) and  $\text{Nb}_2\text{O}_4$  ( $\text{Cu}^{2+}$ ,  $\text{Nb}^{4+}$ ) references. The  $L_{III}$  absorption edge of Nb of the  $\text{Nb}^{4+}$  reference is shifted around 1.2 eV toward lower energies compared to the  $\text{Nb}^{5+}$  reference compound (Fig. 9). The 1000\_1 and 1000\_2 spectra do not exhibit any energy shift compared to that of  $\text{LiNbO}_3$ . This result suggests that the formal oxidation state of Nb remains 5+ after reduction of the doped LN crystals.

Let us examine possible mechanisms for charge compensation. In the case of reduction of all Cu atoms in the 3000\_2\_a crystal (0.3 wt % of Cu), 0.2% of all O atoms should leave the structure for charge compensation (Cu atoms are 1.3% of all Li atoms). The EXAFS analyses suggest that Cu atoms do not share the same oxygen atoms, as no Cu-O-Cu coordination was found (Table III); hence, the number of outgassed O atoms leading to oxygen vacancies should be four times the number of all copper atoms, which is  $\sim 1.7\%$  of all O atoms. Charge compensation for the remaining  $\sim 1.5\%$  O atoms must come through reduction of  $\sim 2.2\%$  Nb atoms from  $\text{Nb}^{5+}$  to  $\text{Nb}^{4+}$ . However, at least 6% of the Nb atoms must have formal oxidation state 4+, in

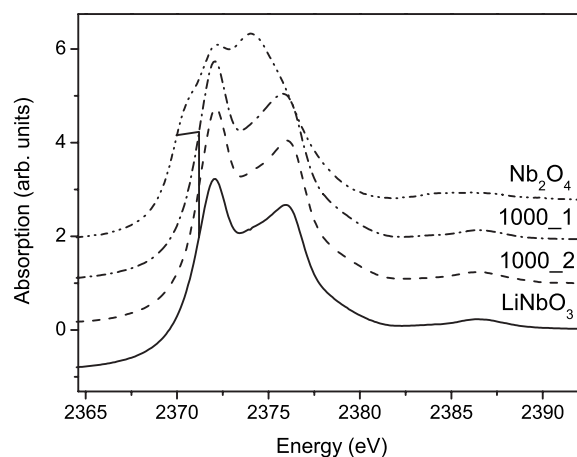


FIG. 9. Nb  $L_{III}$  XANES experimental spectra of the 1000\_1 and 1000\_2 samples and  $\text{Nb}_2\text{O}_4$  and  $\text{LiNbO}_3$  references.

order to shift the Nb  $L_{III}$  XANES spectrum 0.1 eV toward lower energies. The error bar in energy position of the Nb  $L_{III}$  edge is estimated as 0.1 eV, which is the width of one step. Reduction of Nb atoms, theoretically likely, cannot be detected, because the energy resolution is not sufficient.  $\text{Nb}^{4+}$  located at Nb sites has an absorption band at about 1 eV (1240 nm), whereas  $\text{Nb}^{4+}$  located at Li sites has an absorption band at about 1.6 eV (775 nm) so that at least one of these bands should be detected by absorption spectroscopy. However, the  $\text{Cu}^{2+}$  has a broad and unstructured absorption band in the range of 1.2 eV (1040 nm), which lies in the range of  $\text{Nb}^{4+}$  absorption at about 1 or 1.6 eV. The 15% error bar that we assigned to our optical absorption measurements includes also the error due to such absorption bands. One should also keep in mind that we assumed all Cu atoms are reduced from  $\text{Cu}^{2+}$  to  $\text{Cu}^{1+}$ . In reality, none of the crystals in our investigations are reduced completely. From our findings and the corresponding model it is obvious that there are still some discrepancies. Thus, we are planning additional experiments to finally clarify the oxygen problem in  $\text{LiNbO}_3$ .

#### V. CONCLUSION

The XAS studies performed lead to the following conclusions.

(1) The average formal oxidation state of Cu in all samples is between  $\text{Cu}^{1+}$  and  $\text{Cu}^{2+}$  (Table II).

(2) It was found that the average formal valency of Cu does not notably depend on the Cu concentration (for the range 0.1–0.3 wt % of Cu) upon simultaneous diffusion and oxidation of the doped crystals. However, it does depend on the Cu concentration upon reduction of the doped crystals.

(3) We found strong experimental evidence that the Cu atoms occupy predominantly Li sites for all samples. It was possible to distinguish between  $\text{Cu}^{1+}$  and  $\text{Cu}^{2+}$  sites: (i) the  $\text{Cu}^{2+}$  atoms are sixfold coordinated by O atoms in the LN crystals having a formal Cu valence equal to or higher than  $1.7 \pm 0.2$ ; (ii)  $\text{Cu}^{1+}$  atoms are twofold and  $\text{Cu}^{2+}$  sixfold coordinated by O atoms in the LN crystals having formal Cu valence equal to or lower than  $1.5 \pm 0.2$ .

(4) Upon reduction of the doped LN crystals, one of the charge compensation mechanisms is outgassing of O atoms.

(5) No experimental evidence for metal copper or copper oxide cluster formation in the LN matrix was found, even for the highly doped LN crystals (0.3–0.7 wt % of Cu).

(6) Change in the formal oxidation state of the Nb atoms upon reduction of the crystals is likely for charge compensation, but was not detected by the XAS measurements at the Nb  $L_{III}$  edge due to the expected change being lower than the energy resolution.

Understanding of the microstructure of the copper centers, as well as the charge compensation mechanisms during the reduction process, is essential for fine-tuning the optical

properties of copper-doped LN crystals. Moreover, insight into the site symmetry of the impurity centers can help in interpreting the deviations from a perfect Gaussian shape in uv-visible and ir absorption spectra (see, e.g., Ref. 38).

#### ACKNOWLEDGMENTS

The authors gratefully acknowledge financial support for project B1 within the DFG research unit 557. The support by Boris Brendebach, Jörg Rothe, and Kathy Dardenne at the INE beamline is highly appreciated. We also thank Melissa Denecke for critically reading the paper and giving valuable scientific suggestions.

\*vitova@physik.uni-bonn.de

- <sup>1</sup>A. Ashkin, G. D. Boyd, J. M. Dziedzic, R. Smith, A. Ballman, J. Livinstein, and K. Nassau, *Appl. Phys. Lett.* **9**, 72 (1966).
- <sup>2</sup>F. Chen, J. LaMacchia, and D. Fraser, *Appl. Phys. Lett.* **13**, 223 (1968).
- <sup>3</sup>V. Leyva and G. R. B. O’Conner, *Appl. Phys. Lett.* **65**, 1079 (1994).
- <sup>4</sup>S. Breer, H. Vogt, I. Nee, and K. Buse, *Electron. Lett.* **34**, 2419 (1998).
- <sup>5</sup>R. Sommerfeldt, L. Holtmann, E. Krätzig, and B. Grabmaier, *Phys. Status Solidi A* **89**, 106 (1988).
- <sup>6</sup>K. Buse, *Appl. Phys. B: Lasers Opt.* **64**, 391 (1997).
- <sup>7</sup>K. Peithmann, A. Wiebrock, and K. Buse, *Appl. Phys. B: Lasers Opt.* **68**, 777 (1999).
- <sup>8</sup>K. Peithmann, J. Hukriede, K. Buse, and E. Krätzig, *Phys. Rev. B* **61**, 4615 (2000).
- <sup>9</sup>R. Sommerfeldt, R. S. Rupp, H. Vormann, and E. Krätzig, *Phys. Status Solidi A* **99**, K15 (1987).
- <sup>10</sup>A. M. Glass, D. V. der Linde, and T. J. Negran, *Appl. Phys. Lett.* **25**, 233 (1974).
- <sup>11</sup>H. Kurz, E. Krätzig, W. Keune, H. Engelmann, U. Gonser, B. Discher, and A. Räuber, *Appl. Phys.* **12**, 355 (1977).
- <sup>12</sup>E. Krätzig and R. Orłowski, *Ferroelectrics* **27**, 241 (1980).
- <sup>13</sup>K. Peithmann, K. Buse, and E. Krätzig, *Appl. Phys. B: Lasers Opt.* **74**, 549 (2002).
- <sup>14</sup>J. Hukriede, B. Gather, D. Kip, and E. Krätzig, *Phys. Status Solidi A* **172**, R3 (1999).
- <sup>15</sup>D. Kip, B. Gather, H. Bending, and E. Krätzig, *Phys. Status Solidi A* **172**, R3 (1999).
- <sup>16</sup>R. Weis and T. Gaylord, *Appl. Phys. A: Solids Surf.* **37**, 191 (1985).
- <sup>17</sup>S. C. Abrahams and P. Marsh, *Acta Crystallogr., Sect. B: Struct. Sci.* **B42**, 61 (1986).
- <sup>18</sup>P. Marcus, A. V. Chadwick, and A. R. West, *J. Mater. Chem.* **5**, 1043 (1995).
- <sup>19</sup>F. Caccavale, C. Sada, F. Segato, L. Bogomolova, N. Krasil’nikova, Y. N. Korkishko, V. A. Fedorov, and T. Morozova, *J. Mater. Res.* **15**(5), 1120 (2000).

- <sup>20</sup>K. Olimov, M. Falk, K. Buse, T. Woike, J. Hormes, and H. Modrow, *J. Phys.: Condens. Matter* **8**, 5131 (2006).
- <sup>21</sup>M. A. Denecke, J. Rothe, K. Dardenne, H. Blank, and J. Hormes, *Phys. Scr., T* **115**, 1001 (2005).
- <sup>22</sup>M. Lemonnier, O. Coller, C. Depautex, J. M. Esteva, and D. Raoux, *Nucl. Instrum. Methods* **152**, 109 (1978).
- <sup>23</sup>B. Ravel and M. Newville, *J. Synchrotron Radiat.* **12**, 537 (2005).
- <sup>24</sup>J. J. Rehr, J. M. de Leon, S. I. Zabinsky, and R. C. Alberts, *J. Am. Chem. Soc.* **113**, 5135 (1991).
- <sup>25</sup>J. Wong, F. W. Lytle, R. P. Messmer, and D. H. Maylotte, *Phys. Rev. B* **30**, 5596 (1984).
- <sup>26</sup>T. Ressler, J. Wienold, R. E. Jentoft, and T. Neisius, *J. Catal.* **210**, 67 (2002).
- <sup>27</sup>L. Kau, D. J. Spira-Solomon, J. E. Penner-Hahn, K. O. Hodgson, and E. Solomon, *J. Am. Chem. Soc.* **109**, 6433 (1987).
- <sup>28</sup>F. W. Lytle, R. B. Greggor, and A. J. Panson, *Phys. Rev. B* **37**, 1550 (1988).
- <sup>29</sup>K. Shimizu, H. Maeshima, H. Yoshida, A. Satsuma, and T. Hattori, *Phys. Chem. Chem. Phys.* **3**, 862 (2001).
- <sup>30</sup>B. Brendebach, F. Reinauer, N. Zotov, M. Funke, R. Glaum, and H. M. J. Hormes, *J. Non-Cryst. Solids* **351**, 1072 (2005).
- <sup>31</sup>M. Benfatto and S. D. Longa, *J. Synchrotron Radiat.* **8**, 1087 (2001).
- <sup>32</sup>C. Monesi, C. Meneghini, F. Bardelli, M. Benfatto, S. Mobilio, U. Anju, and D. D. Sarma, *Nucl. Instrum. Methods Phys. Res. B* **246**, 158 (2006).
- <sup>33</sup>S. Bocharov, T. Kirchner, G. Dräger, O. Šipr, and A. Šimůnek, *Phys. Rev. B* **63**, 045104 (2001).
- <sup>34</sup>L. Brillouin, *Science and Information Theory* (Academic Press, New York, 1962).
- <sup>35</sup>M. Newville, B. Ravel, D. Haskell, J. J. Rehr, E. A. Stern, and Y. Yacoby, *Physica B* **208–209**, 154 (1995).
- <sup>36</sup>N. Hilbrandt and M. Martin, *J. Phys. Chem. B* **103**, 4797 (1999).
- <sup>37</sup>R. D. Shannon and C. T. Prewitt, *Acta Crystallogr., Sect. B: Struct. Crystallogr. Cryst. Chem.* **25**, 925 (1969).
- <sup>38</sup>U. Hartwig, K. Peithmann, B. Sturman, and K. Buse, *Appl. Phys. B: Lasers Opt.* **80**, 227 (2005).